

Detailed comparison of the structures and kinematics of simulated and observed barred galaxies

J.K. O’Neill^{1,2★} and John Dubinski^{1,2†}

¹*Canadian Institute for Theoretical Astrophysics, University of Toronto, Canada*

²*Department of Astronomy & Astrophysics, University of Toronto, Toronto, Canada*

Received: Accepted:

ABSTRACT

We examine the observable properties of simulated barred galaxies including radial mass profiles, edge-on structure and kinematics, bar lengths and pattern speed evolution for detailed comparison to real systems. We have run several simulations in which bars are created through inherent instabilities in self-consistent simulations of a realistic disc+halo galaxy model with a disc-dominated, flat rotation curve. These simulations were run at high ($N=20M$ particles) and low ($N=500K$) resolution to test numerical convergence. We determine the pattern speeds in simulations directly from the phase angle of the bar versus time and the Tremaine-Weinberg method. Fundamental dynamics do not change between the high and low resolution, suggesting that convergence has been reached in this case. We find the higher resolution is needed to simulate structural and kinematic properties accurately. The edge-on view of the higher-resolution system clearly shows the bending instability and formation of a peanut-shaped bulge. We determined bar lengths by different means to determine the simulated bar is fast, with a corotation to bar length ratio under 1.5. Simulated bars in these models form with pattern speeds slower than those observed and slow down during their evolution. Dynamical friction between the bar and dark halo is responsible for this deceleration, as revealed by the transfer of angular momentum between the disc and the halo. However, even though the pattern speed is reduced at later times, the instantaneous scale length of the disc has grown sufficiently for the bar motion to agree with many observations. By using a different model and simulation technique than other authors, we are able to compare the robustness of these methods. An animation of the face-on and edge-on views of the 20M particle simulation is available at <http://www.astro.utoronto.ca/~oneill>.

Key words: galaxies: kinematics and dynamics – galaxies: evolution – galaxies: haloes

1 INTRODUCTION

The dichotomy between the regular and the barred spirals in Hubble’s original galaxy classification scheme is a long standing problem in galaxy evolution and dynamics. It is unclear what causes a spiral galaxy to become barred or not, or more quantitatively, why barred galaxies represent about 30 to 70 per cent (deVaucouleurs 1963; including weak bars, Sellwood & Wilkinson 1993; viewed in IR, Eskridge et al. 2000) of nearby galaxies. This picture becomes even more confusing at high redshifts, where Abraham et al. (1999)

have found the fraction to drop beyond a redshift of 0.5. Bars undoubtedly form from dynamical instabilities inherent in self-gravitating axisymmetric discs. Early simulations (e.g. Ostriker & Peebles 1973) have shown that purely self-gravitating discs are instantly susceptible to a bar instability, while the addition of a surrounding spheroidal gravitational potential can prevent bar formation; a more recent study suggests this is merely a slow down of formation, and the bar is actually enhanced at later stages (Athanasoulas 2002a). The surrounding stabilizing spheroids can be identified with the dark haloes believed to surround spirals and are responsible for the nearly flat rotation curves of all galaxies. Cold dark matter models of cosmology predict that most spirals are embedded within nearly isothermal haloes (Dubinski & Carlberg 1991; Navarro, Frenk & White 1996,

★ E-mail: oneill@cita.utoronto.ca

† E-mail: dubinski@cita.utoronto.ca

1997). It is therefore useful to examine the consequences of dark haloes on the formation and evolution of barred galaxies to seek consistency with the prevailing world model and the observable universe.

The pattern speed of the bar is an important although difficult to measure indicator of disc dynamics and dark halo structure. Observations of early-type barred galaxies (Merrifield & Kuijken 1995 (M&K); Gerssen et al. 1999) through the application of the Tremaine-Weinberg method (Tremaine & Weinberg 1984b) (T&W) have shown the pattern speed to be ‘fast’, since the bars end near corotation. N-body models of disc dynamics with static background haloes (summarized in Sellwood 1981) have shown the pattern speed also to be fast. However, soon afterward it was recognized (Tremaine & Weinberg 1984a; Weinberg 1985) that rotating bars would spin down significantly due to dynamical friction from the dark halo. More recent simulations with self-consistent disc and halo distributions clearly showed this effect: angular momentum is transferred from the bar to the halo through torques due to gravitational wakes in the halo, which result in surprisingly low pattern speeds for simulated bars (Debattista & Sellwood 2000 (D&S); Misiriotis & Athanassoula 2000). D&S conducted parametric studies by varying the halo to disc mass ratio of their models and found that a maximal disc yields the least pattern speed slow down. They argued that the observational evidence of fast bars implies a maximum disc in all barred galaxies.

Bar structure and dynamics can also be examined in edge-on systems. The thin bars that form in discs are subject to a buckling instability which causes a bar to bend vertically and thicken into a bulge-like object within a few dynamical times, as was shown numerically by Raha et al. (1991), Pfenniger & Friedli (1991), and Combes & Sanders (1981). Kuijken & Merrifield (1995) (K&M) have shown that the kinematics of peanut-shaped bulges of NGC 5746 and NGC 5965 are consistent with orbits in a bar potential, the theory of which was confirmed by Bureau & Athanassoula (1999) (B&A). The observational test described by K&M can also be applied to simulations, which can be viewed at any angle for more complete results.

Through B and I band observations of 15 galaxies, Elmegreen & Elmegreen (1985) have shown that early- (SB0, SBa) and late-type bars have significantly different properties. Although resonance positions and bar lengths are hard to quantify observationally, there is evidence to suggest that early-type bars are longer, out to the corotation radius, have a flat surface brightness profile along their length, and end beyond the turnover radius of the rotation curve. The late-type bars on the other hand are much shorter, with exponential surface brightness profiles.

In this paper, we revisit the problem of the bar and buckling instabilities in self-consistent disc galaxy models with live haloes. Our goal is to study the pattern speed evolution of numerical bars as well as quantify the structural and kinematic properties for comparison with observed face-on and edge-on barred galaxies. We have taken care to re-scale our models to observed systems for comparison. We extend previous work by introducing a new, more realistic mass model and going to much higher resolution with a simulation containing $N=20M$ particles, a factor of 20 times larger than most work on the subject. Our motivation for using high resolution is to examine the numerical conver-

gence of results, since subtleties of dynamical interactions between discs and haloes may not be captured correctly even with haloes with more than $\approx 1M$ particles (e.g. Weinberg 2001). The disc of our large simulation contains $10M$ particles, taking us well out of the regime where disc self-heating contaminates results. We are confident that the dynamics of these models reliably represents the gravitational behaviour of real galaxies. There are also disagreements between various simulations of bars in the literature which use different N-body codes and initial conditions. We attempt here to achieve convergence by comparing three of our simulations with those of other groups, as well as to observations, by examining the bar structure, pattern speed, and edge-on kinematics.

2 MASS MODELS

We simulate bars by setting up an initially axisymmetric system including a disc and dark halo which is formally in equilibrium but unstable. Models with rotation curves which are disc-dominated, approaching the maximal disc as defined by van Albada & Sancisi (1986), usually form a bar within a few dynamical times, and the Ostriker & Peebles (1973) empirical criterion is still a useful indicator of the instability.

We use the method of Kuijken & Dubinski (KD) (1995) to generate self-consistent disc+halo models with a nearly flat rotation curve. We consider models with disc-dominated rotation curves with and without a central bulge. The KD models are generated from a distribution function (DF) that is the sum of up to 3 functions: a three-integral disk DF, a bulge DF modelled as King model with an energy cut-off $E < 0$ and a halo DF that is a flattened King model DF (or lowered Evans model) with the usual truncation at a tidal radius at $E = 0$. We examine models with and without a bulge as described below. The disk DF is a function of E , z -angular momentum, L_z and a third approximate integral, the z energy, $E_z = \dot{z}^2/2 + \Phi(z)$. The disk DF is constructed assuming an exponential radial surface density profile and an approximately $\text{sech}^2 z$ edge-on profile with fixed vertical scale length z_d . The disk squared radial velocity dispersion, σ_R^2 is assumed to decline exponentially with the same scale-length as the disk like real galaxies. We can generate N-body realizations of these models and they are formally in equilibrium with an initial virial ratio $2T/W = -1.0$.

The bulgeless model is nearly a formal maximal disc model, with the rotation curve rising to a roughly flat profile within two scale lengths (Figure 1). Although the halo DF is a King model, the mass profile does not have the usual core since the disk mass dominates the centre. The halo density profile has a mild cusp with $\rho \propto r^{-0.7}$ to within 0.1 disk exponential scale lengths similar to an NFW profile. Whether or not the haloes of spiral galaxies have a central core is still controversial but our model halo here is consistent with rotation curve decompositions (e.g. Kent 1986). The disc is in formal equilibrium with a Toomre $Q \sim 1.1$ measured at $R=2.0R_d$ and is approximately constant in the range $1.0 < R/R_d < 4.0$ rising to higher values beyond these limits. While the model is stable against axisymmetric perturbations it is inherently unstable to bar formation because of the dominance of the disk in the rotation curve. The model is scaled such that $G=R_d=v_{max}=1$, and the to-

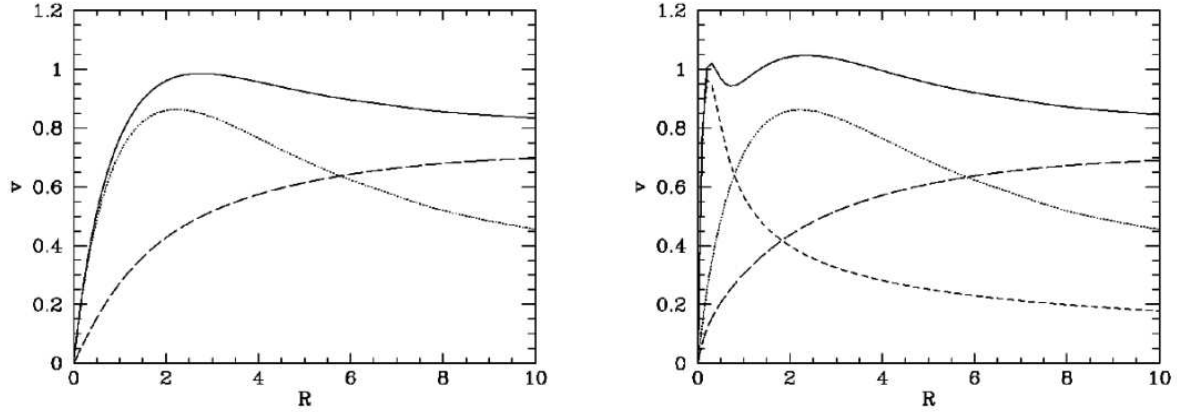


Figure 1. Rotation curves for disc+halo (left) and disc+bulge+halo (right) models in simulation units. The contribution of the disc is shown in dots, the halo in long dashes, the bulge in short dashes and the total as a solid line. R is measured in exponential disk scale lengths.

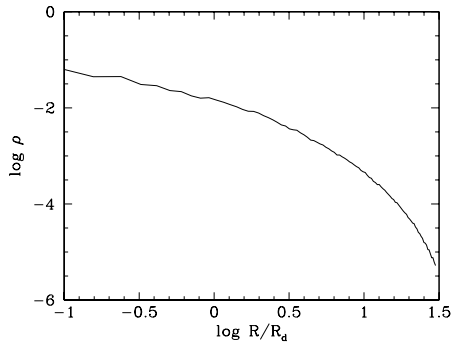


Figure 2. Initial halo density profile: a King model halo with a very small core; the profile is similar to an NFW profile with a -0.7 power law slope until at least $R \sim 0.1$

tal disc+halo mass is about 12 (disc mass of 1.98 and halo mass of 10.57). We realize these models as N-body systems at high resolution with $N=20M$ particles (10M each in the disc and the halo) and low resolution with $N=500K$ particles (250K each in the disc and halo). Thus, all quoted simulation lengths are in terms of the exponential disc length, and all velocities are fractions of the maximum. We also consider a $N=500K$ model with a small compact bulge of mass $M = 0.32$ with halo and disk mass profiles essentially unchanged. The Toomre Q also remains comparable at ~ 1.06 . The code and parameters for generating these models are available by request. Our models differ from D&S who use a Kuz'min-Toomre disc with a vertical Gaussian profile and a lowered polytrope distribution function (DF) for the halo. The recent publication by Athanassoula & Misiriotis (2002) (A&M) contains models based on Hernquist's (1993) method.

As well as specifying the following results in the original simulation units, the appropriate lengths and times are scaled to match the SBa galaxy NGC 4596 for easier comparison with real galaxies. We use the scale length of 3.2 kpc and rotational velocity of 120 km s^{-1} given by Gerssen et al. (1999). The sech^2 scale height for the disc is 0.1 simu-

tion units or 320 pc. For these scales the unit of time is 26.3 Myr. For the runs, we use a time step of $\Delta t = 0.05$ (1.32 Myr) for 10,000 time steps, for a total $t=500$ (13.2 Gyr) or approximately the Hubble time. We soften gravitational forces using a Plummer law with softening length $\epsilon = 0.0125$ (40 pc) for the halo and $\epsilon = 0.005$ (16 pc) for the disc. All runs are executed with a parallel tree code (Dubinski 1996) running on a PC cluster or a 32 processor Compaq GS320. The 20M particles simulations needed 2 minutes per step on the GS320. The total energy drifts by no more than 1 per cent, and total angular momentum is conserved to typically within 0.1 per cent. The results discussed below are for the high resolution simulation unless otherwise noted.

3 BAR FORMATION AND STRUCTURAL EVOLUTION

Although these models are formally in equilibrium they are strongly unstable. A bar develops by $t=26$ (686 Myr), and is sustained for the duration of the run. Visually, the bar grows to its greatest extent at around $t=50$ (1.32 Gyr). The bar then bends and buckles between $t=70$ and $t=90$ (a period of 526 Myr) to leave a slightly slower bar of comparable length. There are isophotal twists seen during the bar buckling phase, but as noted in Shaw et al. (1993) these disappear with the increased heating of the disc seen during the bar evolution. After this short phase, the bar shows elliptical isophotes with a butterfly- or dumbbell-shape when viewed face-on. Fig. 3 shows the face-on views for $t=50$ to 500.

The evolution of the bar viewed edge-on clearly reveals the buckling instability. Initially the disc is thin; the formation and motion of the bar heat the disc vertically and azimuthally. At the onset of buckling there is a very short lived phase of about 260 Myr in which the bar bends into an arc before buckling into a boxy shape object (edge-on views are shown in Figs 4 and 5). The boxy-shaped bulge remains after buckling, and slowly evolves into the familiar peanut shape, which is most prominent when the bar is viewed edge-on, with its long side in the plane of the sky.

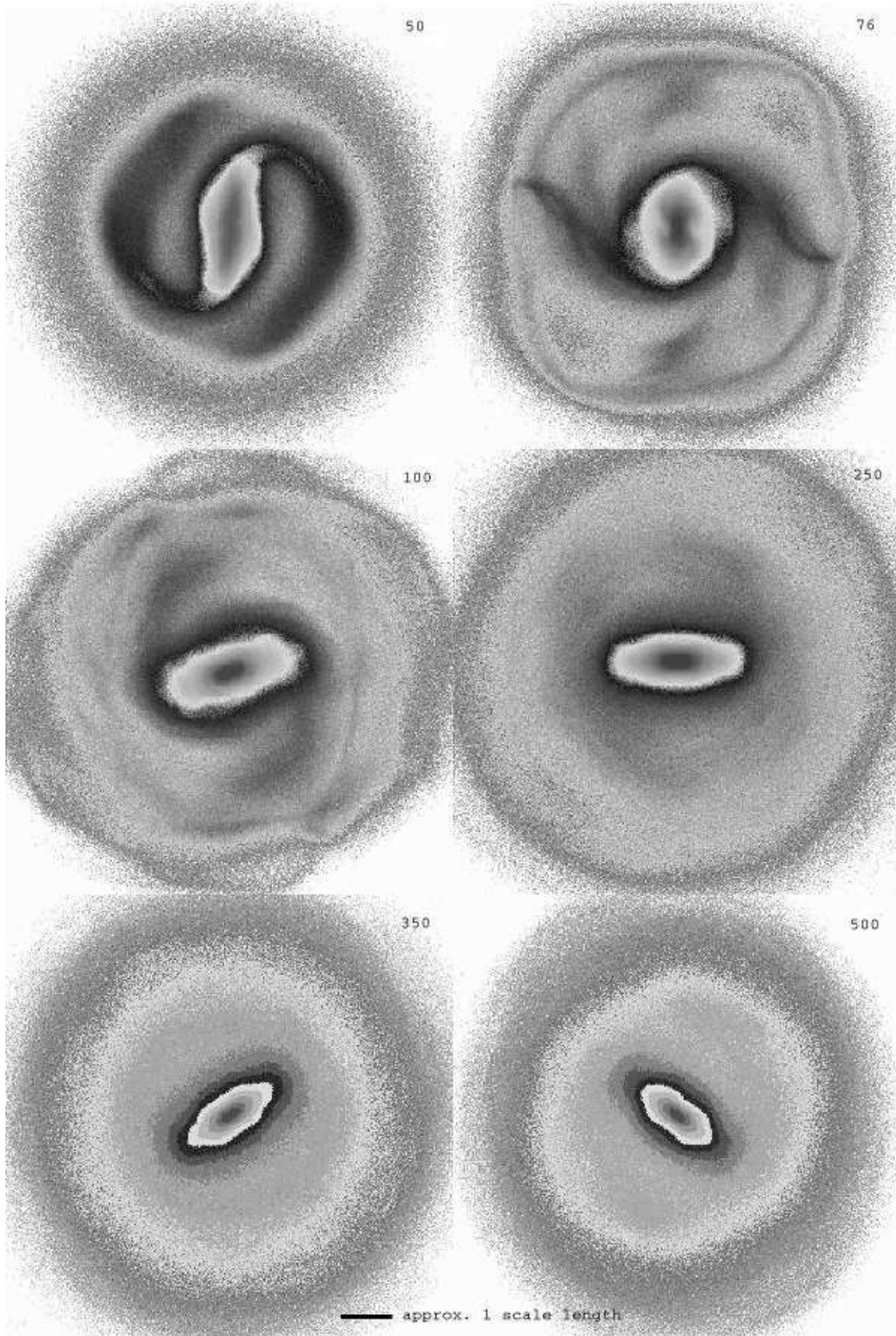


Figure 3. Logscale density diagrams of the face-on views of the simulated galaxy at $t=50$, 76 , 100 , 250 , 350 , and 500 .

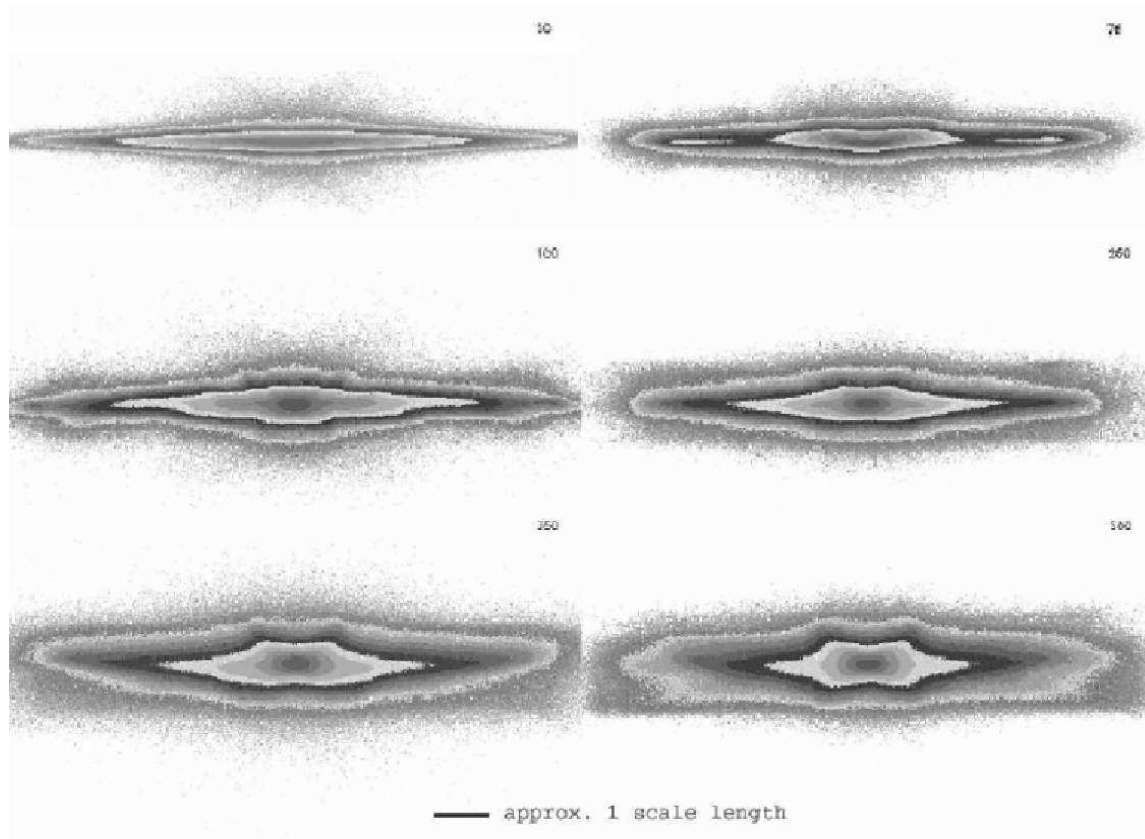


Figure 4. Logscale density diagrams of the edge-on views of the simulated galaxy at $t=50$, 76 , 100 , 250 , 350 , and 500 .

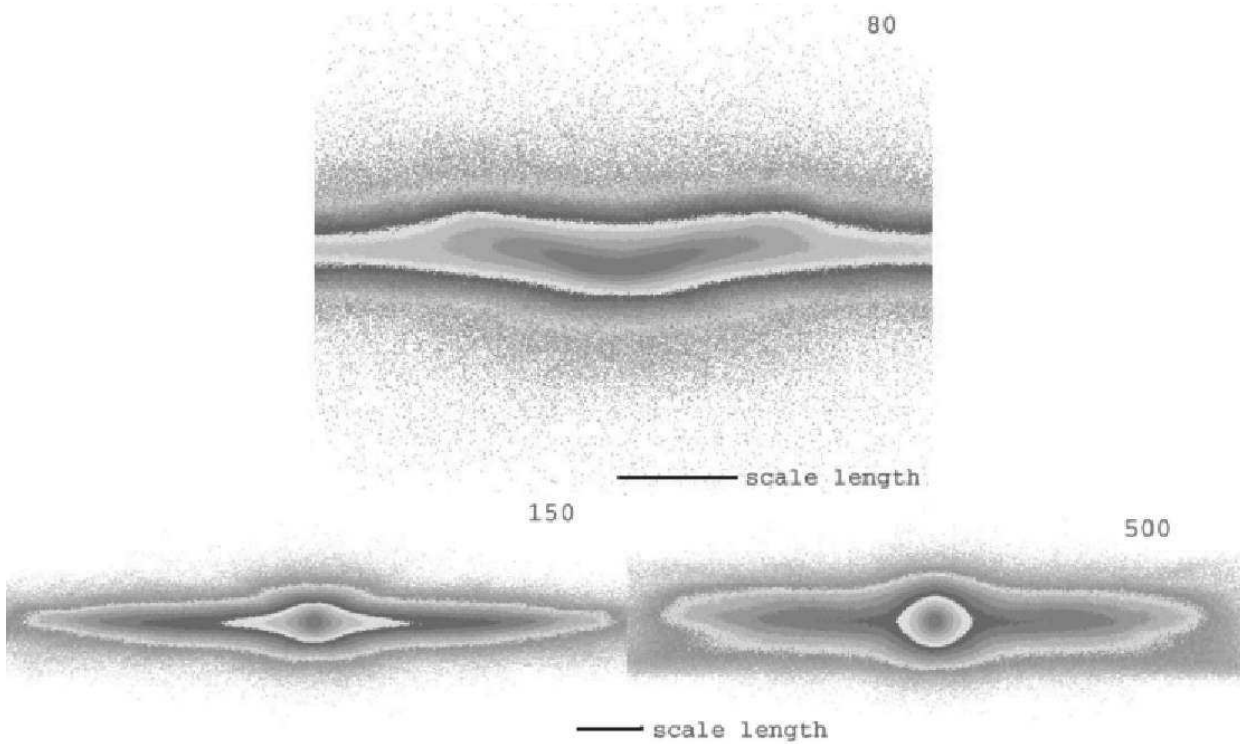


Figure 5. The edge-on views of the simulated galaxy showing the warp at $t=80$, and the end on views of the bar at $t=150$ and 500 .

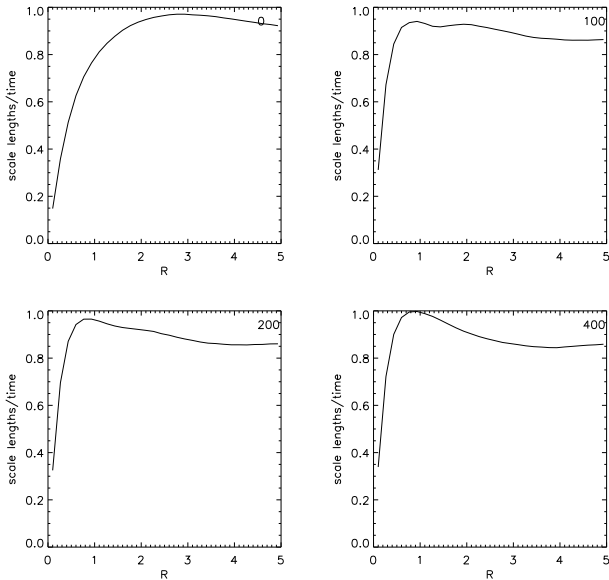


Figure 6. Rotation curve of the simulated galaxy at $t=0$, 100, 200, and 400. The bar causes an increase in central mass, which increases the initial slope of the rotation curve as well as raising the maximum value.

When viewed end-on, the galaxy resembles a disc with a spherical bulge. The bar remains an obvious component of the disc and shows no sign of collapsing into a spherical bulge. There is an animation of both face-on and edge-on views available at www.astro.utoronto.ca/~oneill.

There is an increase in central density following the initiation of the bar, which influences the initial slope of the rotation curve. Fig. 6 shows the rotation curve at $t=0$, 100, 200, and 400, and it shows the increased slope and peak during the simulation. The surface density along the bar is flat at small R for $t=50$, but rapidly turns exponential following buckling. These data will be discussed in more detail in the following sections.

Even without the gaseous component, this simulated galaxy can be compared with observations, and some obvious features stand out. The face-on views look very much like observed bars, and the edge-on views are similar to several studies comparing peanut-shaped bulges and bars (K&M; Merrifield & Kuijken 1999). More detailed comparison with the latter follows in Section 5.

Recently, A&M conducted a series of tests to compare N-body simulations of different mass models, which are ideally suited to comparison with our results here. They simulated three different models: one disc-dominated (MD), which is similar to ours here, another disc-dominated model with an added bulge (MDB), and one halo-dominated (MH): all created using the Hernquist (1993) models.

Our work agrees quite well with A&M on isophote shape and rotation curve progression for the first half of the simulations, which span approximately the same time. Our evolution here disagrees to some extent with their disc dominated model for the latter half of the run: the mass build up at the centre of the disc causes the inner slope of the rotation curve to become more steep (albeit slightly) and the maximum velocity to increase even during the final stages; whereas, A&M found little difference between the rotation

curves for the last quarter of their run. This also carries over to the bar isophote structure, as our increasing central density causes the bar shape to become similar to their MDB model. Therefore, the latter half of our simulation is more readily compared to dumbbell-shaped, face-on and peanut-shaped, edge-on isophotes, which they produce with the MDB model. Our low-resolution model, with a similar number of disc particles as were used by A&M, shows only boxy isophotes, but was run for half as long as the high-resolution model. Since the buckling stage was later in this simulation, the evolution into a peanut-shaped bulge would be expected after the end of the simulation, so it is uncertain whether we would agree with A&M in this case or not. The rotation curve for our low-resolution model does not change slope for the last 100 simulation time units, which may suggest that the mass redistribution does not continue as long as the high-resolution model run.

We also investigated the evolution of the halo. Unlike Weinberg & Katz (2002), the central density distribution of our halo remained virtually unchanged. There were several differences between our models which may account for this. (1) Their bars were much stronger than ours (30 per cent of the disc mass), appearing earlier in the formation of the galaxy out of a cold, gaseous disc (ours formed in the stellar disc of a galaxy initially in equilibrium), which will have a greater dynamical friction effect on the halo. (2) Our halo is based on the King model, which according to Weinberg & Katz (2002) is missing the key resonance for redistributing the halo mass. However, the KD models are composite DFs and the resulting halo has a mild cusp with an effective power law slope of -0.7 at the centre, which is similar to an NFW profile. (3) They stress the need for high resolution, using 4M particles in the halo; they are concerned that tree codes induce more small scale noise and require higher resolution – they did not outline how much more, but the 10M particles in our halo should be enough to see some indication of halo density redistribution.

4 BAR PATTERN SPEED

T&W describe the only method available to measure pattern speeds of real galaxies from observable quantities alone. This method uses luminosity, line-of-sight velocity, and tilt angle to determine the rotation rate of the bar. To date there have been a few early-type galaxy bars measured this way, and every one of them has been found to be fast, with the corotation distance to bar length ratio between 1 and 1.5. This result has been difficult to reproduce in simulations, as all the bars are greatly slowed due to dynamical friction between the bar and the halo. The amount of mass in the halo compared with the disc is still a point of contention, because the existence of a flat rotation curve constrains, but does not pinpoint, this ratio. Studies on this relation refer to ‘maximal’ or ‘sub-maximal’ discs, where the former has the largest disc to halo mass ratio in the inner regions of the disc that is consistent with observed rotation curves (van Albada & Sancisi 1986). D&S used the dynamical friction between the bar and halo to show that only a maximal disc is likely in barred galaxies, since these bars slow down the least. The final state of their maximal disc simulation was

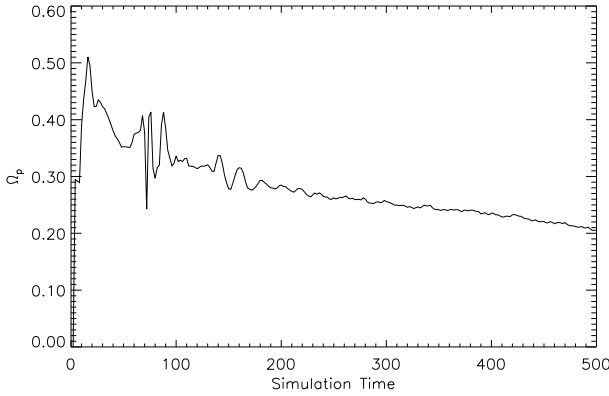


Figure 7. Pattern speed of the bar vs. simulation time units (rad t^{-1}): the pattern speed continues to slow even after a Hubble time.

nearly a fast bar, with a corotation to bar length ratio of 1.6 ± 0.3 .

We used two different methods to determine the pattern speed of the bar (Ω_p). The first was a direct measurement of bar rotation by determining the orientation angle of the bar as a function of time. Fig. 7 is a plot of pattern speed versus time in the original simulation units. Early on, the pattern speed is 0.44 at $t=26$ but there is a rapid reduction during the initial bar growth, and by $t=50$ it has slowed to 0.35, then there is another drop during the buckling phase from $t=65$ to 95, with the pattern speed settling to 0.33 (the following section compares these with observations). After that initial phase of rapid evolution, the pattern speed is influenced by dynamical friction, as it gradually slows to less than 0.21 by the end of the simulation. Even after approximately a Hubble time, it does not reach a steady state; it is still transferring angular momentum to the halo (see Fig. 8). We note in Fig. 7 that the pattern speed shows significant scatter early on, during bar formation and buckling phases. After formation, the pattern speed smoothly, but quickly, decreases. During buckling, the scatter is probably due to difficulty in precisely measuring bar position in the midst of twisted isophotes. There is also a series of oscillations which continue after the buckling phase which we believe to be real, whose period corresponds to slightly more than the circular period of the disc at corotation. We are uncertain at this time of the cause of these oscillations.

In order to compare these results with both observations and other simulations, they must be scaled to comparable units. We have taken the R (scale length) divided by v (circular velocity) to determine a scaling factor (DS subscripts for Debattista & Sellwood, OD subscripts for O’Neill & Dubinski):

$$\frac{\Omega_{pDS}}{\Omega_{pOD}} = \frac{v_{DS}}{v_{OD}} \times \frac{R_{OD}}{R_{DS}}. \quad (1)$$

In comparison with the maximal disc simulation (run 68) from D&S our scaled pattern speed is slightly lower than theirs for the duration of the simulation, 0.086 rad t^{-1} instead of about 0.1 after the bar is fully formed, and 0.054 rad t^{-1} instead of around 0.057 at the end of our simulation. Although certainly disc dominated, our mass model would be more correctly compared with D&S control run, which has a similar disc to halo velocity ratio (their η pa-

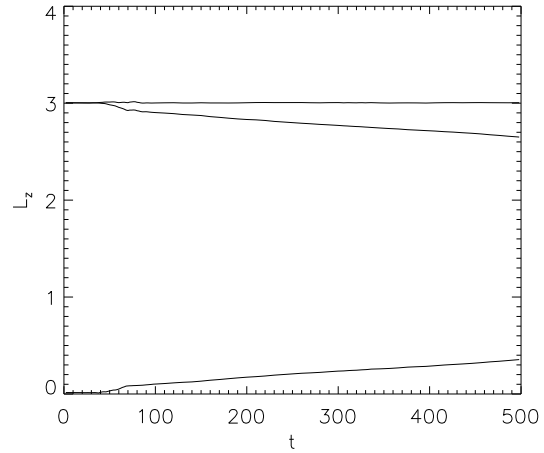


Figure 8. Angular momentum of the disk (middle), halo (bottom), and total (top). The total angular momentum is well conserved and there is a transfer of 10% of the disk angular momentum to the halo.

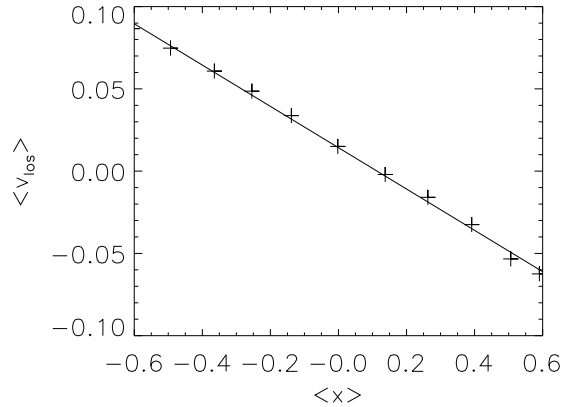


Figure 9. Determining pattern speed (slope) from luminosity-weighted velocity over position.

rameter). Here, our bar pattern speed is slower initially (0.093 rad t^{-1} instead of around 0.15), but does not slow down as quickly or as much as their simulation (final speed 0.058 rad t^{-1} instead of around 0.041). Because we are using different simulation techniques and mass models, the agreement here is promising, although it should be noted that our pattern speed degradation is consistently lower than D&S. This agrees with Athanassoula’s (2002b) assertion that bars slow down at a faster rate in colder disks.

We also measured the bar pattern speeds using the observational technique described by T&W. Taking observations from multiple slits laid parallel to the apparent major axis of the tilted disc and finding the luminosity-weighted position and average line of sight velocities determines the pattern speed:

$$\Omega_p \sin(i) = \frac{\langle \overline{v_{los}} \rangle - v_o}{\langle x \rangle - x_o} \quad (2)$$

(M&K). This method, although direct, is not simple to execute observationally. Since the basis of this relation is the continuity equation, common observations using gaseous

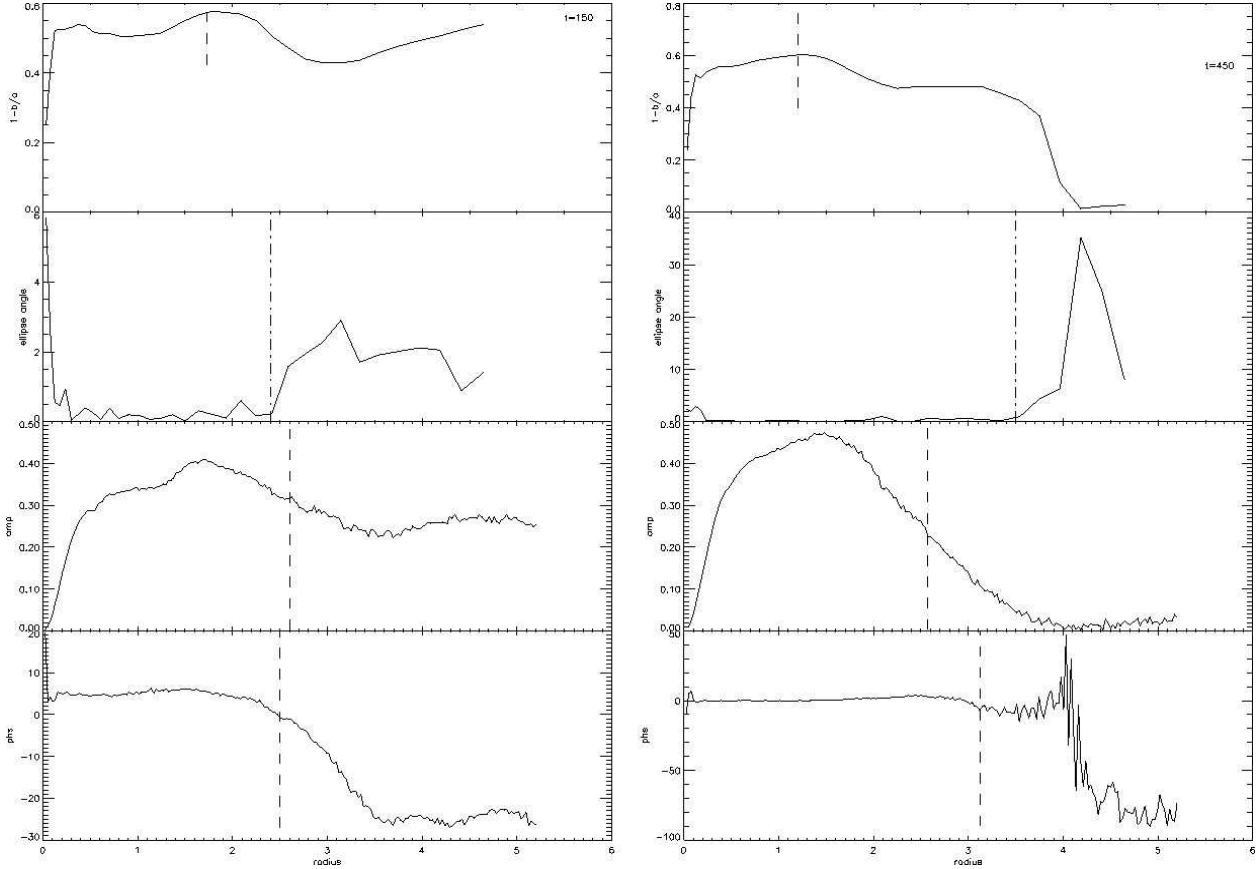


Figure 10. Four methods of determining bar length: ellipticity of the bar ($1 - b/a$) - the point where $1-b/a$ is a maximum corresponds to the end of the bar; phase angle of the ellipses - where the angle deviates 5 deg; $m=2$ Fourier amplitude and phase; the bar end is measured halfway down the slope on the amplitude plot, and where the phase plot deviates by 5 deg. $t=150$ and $t=450$ are shown with the dashed line indicating the measured bar length for each method.

emissions are disqualified, as the gas cycle through stars is inherently discontinuous. The method is therefore most accurate for those early-type barred spiral galaxies with the least amount of gas and star formation. There are also preferred tilt angles to the galaxy to minimize error and difficulties surrounding determining the line-of-sight velocities. It does, however, remove many of the uncertainties inherent in the indirect methods.

Conversely, this technique is relatively simple to perform on simulated data. At various points during the simulation, snapshots were rotated so the bar was at a 45° angle to the x-axis, then tilted about this axis by 30° , similar to the observed galaxies listed below. Slits were laid through the centre of the nucleus and at ± 1 scale length, parallel to the major axis. Fig. 9 plots the luminosity weighted velocity versus position, with the assumption of a constant M/L ratio.

This method works very well with the simulated galaxy, with speeds agreeing to within around 2 per cent of actual for the duration of the simulation when using the known 30° inclination of the disc. However, in observational analysis the tilt of the galaxy is not known, and these simulations show that the outer isophotes of face-on systems are not exactly circular. Therefore, determining the tilt of the galaxy by assuming this regular shape will lead to errors. Based on the distance to NGC 4596, the outermost detectable isophote is

at 5.8 scale lengths. At $t=200$ (5.4 Gyr), the axis ratio b/a at this radius is 0.72. If assumed circular, the computed tilt angle would be 44.2° instead of 30° , which would result in a 26 per cent error on the pattern speed as opposed to the 2.6 per cent error found with the correct inclination. These errors systematically underestimate the pattern speed and are reduced as time progresses and the outer isophotes become more regular with the disappearance of any spiral pattern or time-dependent instabilities.

The definition of a fast or slow bar depends on the length of the bar and the positions of the resonances. The former is a point of contention. A&M have shown that any one method of determining bar length will not work equally well for the duration of the galaxy's lifetime. In this paper we use several methods to determine the length of the bar: the radius where the phase angle of the elliptical isophotes twists, the $m=2$ component of the Fourier amplitude and the $m=2$ phase component. The latter two are used by D&S, and all three are used observationally by Aguerri et al. (2003). Originally we had attempted to use Abraham et al.'s (1999) description for finding the bar length by choosing the elliptical isophote with the smallest b/a axis ratio (option (i) or $L_{b/a}$ in A&M's comparison of bar length determination methods), but we found this method consistently underrepresented the bar in comparison to the other methods. A large drop in this measure during the last third of the simulation

causes the difference to jump from around 25 per cent to 60 per cent shorter, although we find similar ellipticity plots as A&M for their MD model, where the $1-b/a$ measure reaches a peak before the end of the bar, then gradually declines. The peak occurs at a smaller radius for the later time steps. The first three methods and the resulting bar length determination from each are plotted in Fig. 10. Fig. 11 shows the average bar length using the first three methods as a function of time, with error bars corresponding to the maximum and minimum lengths calculated. The bar length appears to be constant or slightly increasing with time. Also plotted are the corotation to bar length ratios, which are all under 1.5, indicating the bar is fast throughout the galaxy's evolution. D&S quote a final corotation to bar length ratio ($D_L : a_b$) of 1.57 ± 0.27 which they call 'acceptably fast ... only barely so'. There is some agreement between our results and theirs, especially if we only take the Fourier component methods into account, where we find a final ratio of 1.44 ± 0.1 .

4.1 Comparison with observations

The actual pattern speed of the bar is scaled to the dimensions of real galaxies and compared with observed pattern speeds listed in Table 1.

The T&W method directly measures pattern speed from observables, and is thus more accurate than the other, indirect, methods. It has thus far only been applied to a handful of galaxies, most of which are listed in Table 1. The T&W method depends on continuity, which the life-cycle of gas inherently contradicts, so reliable use of this measurement is restricted to early-type galaxies.

The scaled pattern speeds found in this simulation are initially too slow for all but one galaxy (although two more are just barely within the lower bound of the observed error bars). However, even though the pattern speed decreases with time, the redistribution of the disk particles by the bar causes the scale length of the disk to increase with time as well. Measured with a double exponential fit to the surface density profile, this increase in the disk scale length is fairly rapid initially, jumping to 2.3 from 1.0 between $t = 50$ and $t = 110$, and slowly increasing to 2.8 by the end of the simulation. This increase more than offsets the pattern speed slow-down, with only one comparison still too low at $t = 110$ while two are higher than observed, and the rest are within the accepted ranges. By the end of the simulation three are again too low, only one is too high, and the rest are acceptable (with two at the lower limit of the error bars, and two well within the measured range). Therefore, for a considerable duration, these long-lived bar is rotating at speeds comparable to those observed. This reiterates the corotation to bar length ration finding above: both the simulated and observed bars are "fast" (ratio less than 1.5).

5 EDGE-ON KINEMATICS

Some attention has recently been placed on the identification of edge-on barred galaxies. K&M, Athanassoula & Bureau (1999) (A&B), and B&A have studied the line-of-sight velocity profile of peanut-shaped, edge-on galaxies and have shown that their kinematics are explained by the presence

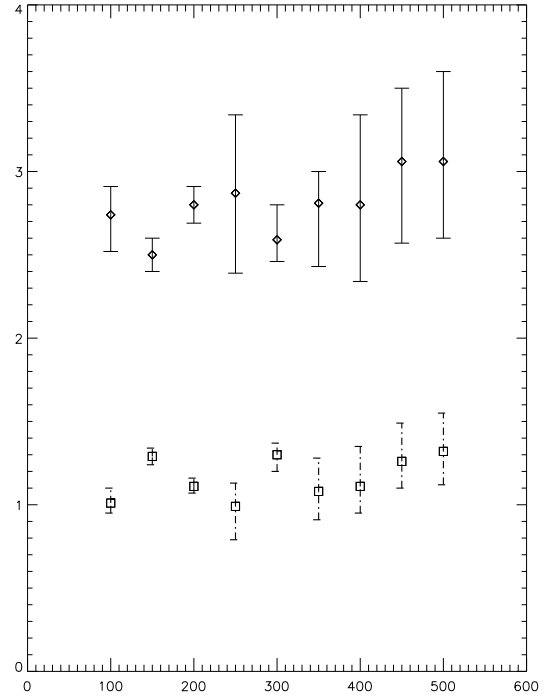


Figure 11. Bar length (triangles) determined by the average of three techniques plotted in Fig. 10 (ellipse angle, $m=2$ Fourier amplitude and phase; ellipticity was found not to be a good indicator in this case). Corotation to bar length ratio is noted with squares at the bottom of the plot; the ratio is always below 1.5, indicating a fast bar.

of a bar. The characteristic plot of position versus velocity gives a unique figure-eight pattern for barred galaxies, since some orbits are depleted in these systems. Our simulation results have been similarly plotted. After initial bar formation, the plot appears similar to the unbarred plots; as the bar develops, the central positions darken while the density increases, and the areas immediately to the outside of this central pole suffer some depopulation, similar to the observational plots in K&M and A&B. With bar buckling, though, comes increased scatter in the plot, removing any forming pattern, and once again leaving a plot which would be considered unbarred if viewed observationally. Plots at $t=50$ and $t=76$ are shown in Fig. 12.

The original simulation is composed only of a disc and halo and was constructed to be in equilibrium with a Toomre Q greater than 1. This generates a higher velocity dispersion than would be observed: 0.23 (times maximum velocity) tangential and 0.215 radial dispersion at 2.4 scale lengths. The radial dispersion increases to 0.258 by $t=76$. This blurs the figure-eight pattern in the K&M plot. Since all the observational results used cool gas to determine velocities, our results would be much closer to the analytically predicted orbits, and the distinctive figure-eight plot.

6 BULGE MODEL

To counter part of the possible velocity dispersion problem stated above, a model containing a small, compact bulge was

Table 1. Comparison of simulated and observed pattern speeds.

Galaxy	R_e (kpc)	Velocity (km s ⁻¹)	Obs. Ω_p (km s ⁻¹ kpc ⁻¹)	Sim Ω_p (t=26) (km s ⁻¹ kpc ⁻¹)	Sim Ω_p^* (t=110) (km s ⁻¹ kpc ⁻¹)	Sim Ω_p^* (t=500) (km s ⁻¹ kpc ⁻¹)
NGC 4596 (SBa) ^a	3.2 ^b	120 ^b	52 ± 13	16.4	27.38	21.6
NGC 936 (SB0) ^c	3.5 ^d	280 ^d	60 ± 14	35	58.4	46
NGC 1023 (SB0) ^e	2.9	270	87 ± 30	40.7	68	53.6
ESO 139-G009 (SAB0) ^f	4.1 ^g	314	61 ± 17	33	55	44
IC 874 (SB0) ^f	1.88 ^g	187	41.6 ± 14.3	43	73	57
NGC 1308 (SB0) ^f	3.6 ^g	347	99.4 ± 34.8	43	71	56
NGC 1440 (SB0) ^f	1.7 ^g	283	83 ± 10	74	124	98
NGC 3412 (SB0) ^f	2.2 ^g	205	57 ± 16	42	69	55

*Determined with instantaneous scale length (at t=110, $R_e=2.3$ and at t=500, $R_e=2.8$)

^a Gerssen et al. 1999

^b Galaxy properties from Kent 1990

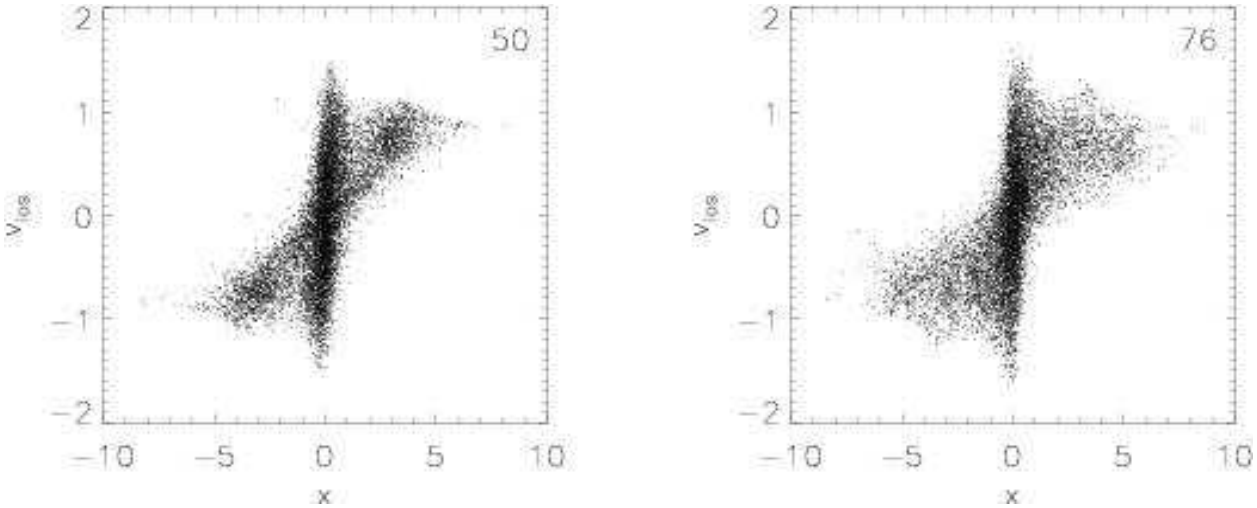
^c Merrifield & Kuijken 1995

^d Galaxy properties from Kent 1989

^e Debattista et al. 2002

^f Aguerri et al. 2003

^g Debattista, private communication

**Figure 12.** Line-of-sight velocity distributions from t=50 and t=76. A slight figure-eight pattern is emerging at t=50, but is wiped out by the buckling phase at t=76.

constructed in the lower resolution range (500K particles), keeping a similar halo and rotation curve (see Section 2 for a more complete description). The evolution of the disc is similar to the earlier model in that the bar is initiated a little before $t=20$ (540 Myr); it differs in that the initial bar is about 20 per cent smaller, with dumbbell-shaped inner isophotes when viewed face-on. The bar remains smaller than the the previous model, by about the same amount for the duration of the simulation. This is in direct contrast with the findings of A&M who found their bulge model to have a longer bar, although the shape is similar. However, their bulge is more massive in comparison to the disk, and more extended than ours. Fig. 13 shows $t=26$ to 250. The initial velocity dispersion (0.146 versus 0.23 above for tangential and 0.18 versus 0.215 for radial) was lower than our original simulation; however, the line-of-sight velocity distribution (LOSVD) plots remained similar. The high resolution simulation showed much more detail and followed trends toward the figure-eight shape not seen in the lower resolution plots

for the same initial conditions. Creating a simulation of the bulge mass model with higher resolution, with its lowered velocity dispersion, should yield clearer LOSVD plots than the original high resolution run, therefore we cannot make any conclusions as to whether or not the inflated velocity dispersion in the original simulation is responsible for masking the figure-eight pattern.

The pattern speed of the bulge model is higher than the original for the duration of the simulation, is reasonably steady after $t=100$ and can be compared with observations, as earlier. The result is that the pattern speed scales up to an acceptable rate for NGC 1023, ISO 139-G009, and NGC 1308, is too low for NGC 4596, and too high for NGC 936, IC 874, NGC 1440, and NGC 3412 for the whole run. The final measured pattern speed for the bulge model (at $t=250$) is the same as that for $t=50$ in the original disc+halo model. Some speed increase is to be expected with the higher central density, as was mentioned in D&S; however, too much central density means the disc is no longer unstable to bar

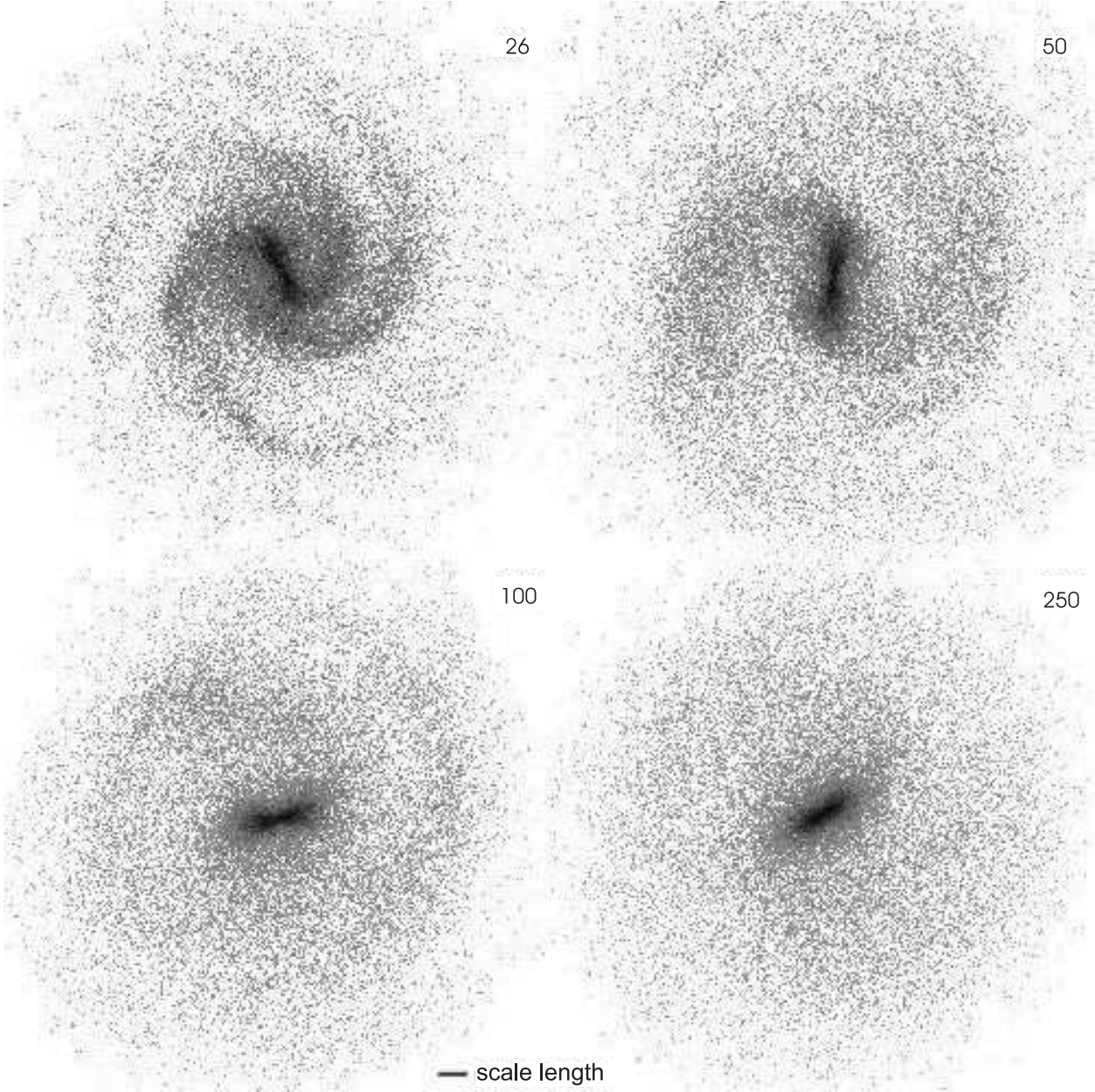


Figure 13. Non-contoured logscale face-on views of the bulge model for $t=26$, 50, 100, and 250. Only the disk particles are shown.

formation. The bar was even closer to corotation, with a D_L/a_B of near one for most of the run, ending with $1.3 \pm_{0.17}^{0.33}$.

7 HALO BAR

A slightly elongated shape was excited in our halo, with an axis ratio of around 0.88. If the alignment of this halo bar were to coincide with the disc bar, the dynamical friction should be reduced. Although the Ω_p deceleration slows after about $t=150$, suggesting a decrease in torque on the bar, the halo bar takes much longer to line up with the disc bar. The bar orientations are mostly within 10° of one another after $t=450$, although not locked in at the same relative angle. D&S also found an $m=2$ response in the halo which slowly aligns with the disc bar.

The pattern speed degradation during the later time steps may not be solely due to the halo friction. Misiriotis & Athanassoula (2000) have shown that the Ω_p is slower in thicker discs. As the bar buckles and the simulation progresses, the scale height of the disc increases. This should then also slow the bar, even if the halo bar is locked into synchronous rotation with the disc bar, and the dynamical friction between the disc and halo is at a minimum.

8 COMPARISON OF EARLY AND LATE TYPE BARS

Elmegreen & Elmegreen (1985) studied the kinematic and dynamic properties of different Hubble-types. They found distinct photometric differences between early (SB0-SBbc)

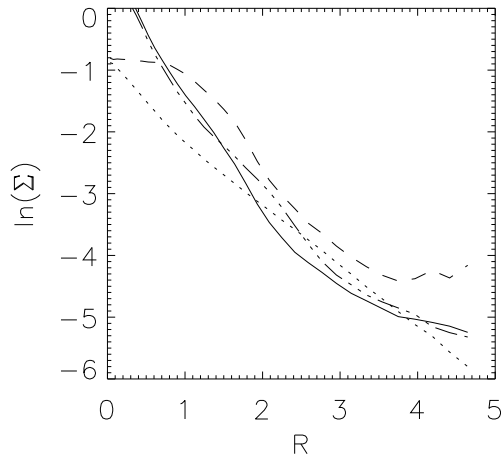


Figure 14. Surface density (luminosity) for $t=0$ (dotted), $t=50$ (dashed), $t=250$ (dash-dot), and $t=500$ (solid). $t=50$ shows an initial flat-topped profile, but the flat section is about half the length of the bar. The later times show an evolution to a double exponential.

and late-type galaxies. Early-type galaxy bars appear to end at or near corotation and are twice the length of the turnover radius of the rotation curve. Their luminosity profile is flat compared with the exponential decrease of the rest of the disc. Late-type bars are shorter, seem to end near the inner Lindblad resonance, and are shorter than the turnover radius. They have an exponential luminosity profile with a different slope than that of the disc.

The properties of the bar evolves during our simulation. By assuming a constant M/L , the density profile of the bar can be taken as representative of a luminosity profile (Fig. 14). Soon after the bar forms, a small section of the bar near the core has a flat density profile, with a near exponential decrease for the remainder of the bar. Later time steps show only exponential profiles. The bar length is near the corotation resonance for the duration of the run, and the bars are always longer than the turnover radius and the inner Lindblad resonance. Fig. 15 contains plots of the Lindblad resonances for the bar: Ω , $\Omega - \kappa/2$, and $\Omega + \kappa/2$, which are determined based on an azimuthally averaged redistribution of the particles to make the disk axisymmetric. The bar length criteria agree with an early-type galaxy, but the density profile is late-type. Another point to note is that early-type galaxies are also characterized by a large bulge to disk ratio, whereas our models, at most, have a very small bulge.

The main results we are comparing in this study (evolution of pattern speed, corotation to bar length ratio) may actually be similar for all barred galaxies. Kinematical studies have shown that bars should be fast even in late-type galaxies (e.g. due to dust lane placement Athanassoula 1992, and hydrodynamical simulations Weiner et al. 2001). Therefore, our small or no bulge galaxy with fast bar with an exponential density profile is fully consistent with a real late-type galaxy.

9 DISCUSSION

9.1 Resolution

Along with the 20M particle simulation, a 500K particle run with the same initial conditions was conducted for comparison. The pattern speed is very similar, although after $t=350$ the lower resolution model slows a little more than quoted above ($\Omega_p = 0.18$ vs. 0.20). The bar lengths, based only on the $m = 2$ amplitude and phase change, are in general shorter than in the 20M simulation before $t=350$, and longer thereafter, showing a distinct trend to increasing the bar length over time. Most of the values are within the error bars of Fig. 11, and there is therefore at least in nominal agreement between the two simulations.

The high resolution simulation showed much more detail in the bar. For example, isophote twists during the formation and buckling of the bar were clearly seen, whereas they were absent in the lower resolution model. The T&W method of finding pattern speed was also more accurate with the larger number of particles. The 500K model results were within 5-10 per cent of the actual pattern speed as opposed to around 2 per cent for the high resolution results.

By the midpoint of the runs, scale height calculations were comparable with the original simulation, but at $t=100$ the average scale height for the high resolution simulation seems to be higher than the 500K model. This is most probably due to the fact that the bar in the high resolution simulation has already buckled at this point, whereas the low resolution model has not; buckling heats the disc. The scale height is of some interest, as it shows the interaction of the bar with the disc, and an increased scale height has been shown to decrease the pattern speed (Misiriotis & Athanassoula 2000).

Therefore, it can be concluded that the lower resolution is capable of outlining many dynamical properties, but higher resolution is needed for some detailed comparisons with real galaxies.

9.2 Code Comparison

Victor Debattista and Jerry Sellwood generously offered the use of their mass model initial conditions to run in our simulation code for comparison. Their simulation was run using a 3-D Cartesian particle-mesh code, with a grid spacing of $0.2R_d$, and a total particle count of 600K (102K in the disc). Here we run the same particles (run 68 in D&S, maximum disc model) with a tree code (Dubinski 1996). We initially had problems with our small softening length, until we changed this to correspond with the grid resolution in their original simulation (equivalent to a Plummer softening of 0.4 scale lengths (1.3 kpc) instead of 0.0125 for the halo and 0.005 for the disc), as their particles are set up in equilibrium with respect to the mesh. They ran many different initial conditions during their research, and we found the $Q=1.5$ model (unpublished) to evolve similarly to our code. We found a pattern speed of $0.095 \text{ rad } t^{-1}$ at $t=1000$ compared to around 0.07 plotted in their paper (their units), and a shorter bar than the original, although when Debattista and Sellwood (private communication) ran the same model in a higher resolution mesh code this result was corroborated. The equilibrium of the particles with the original

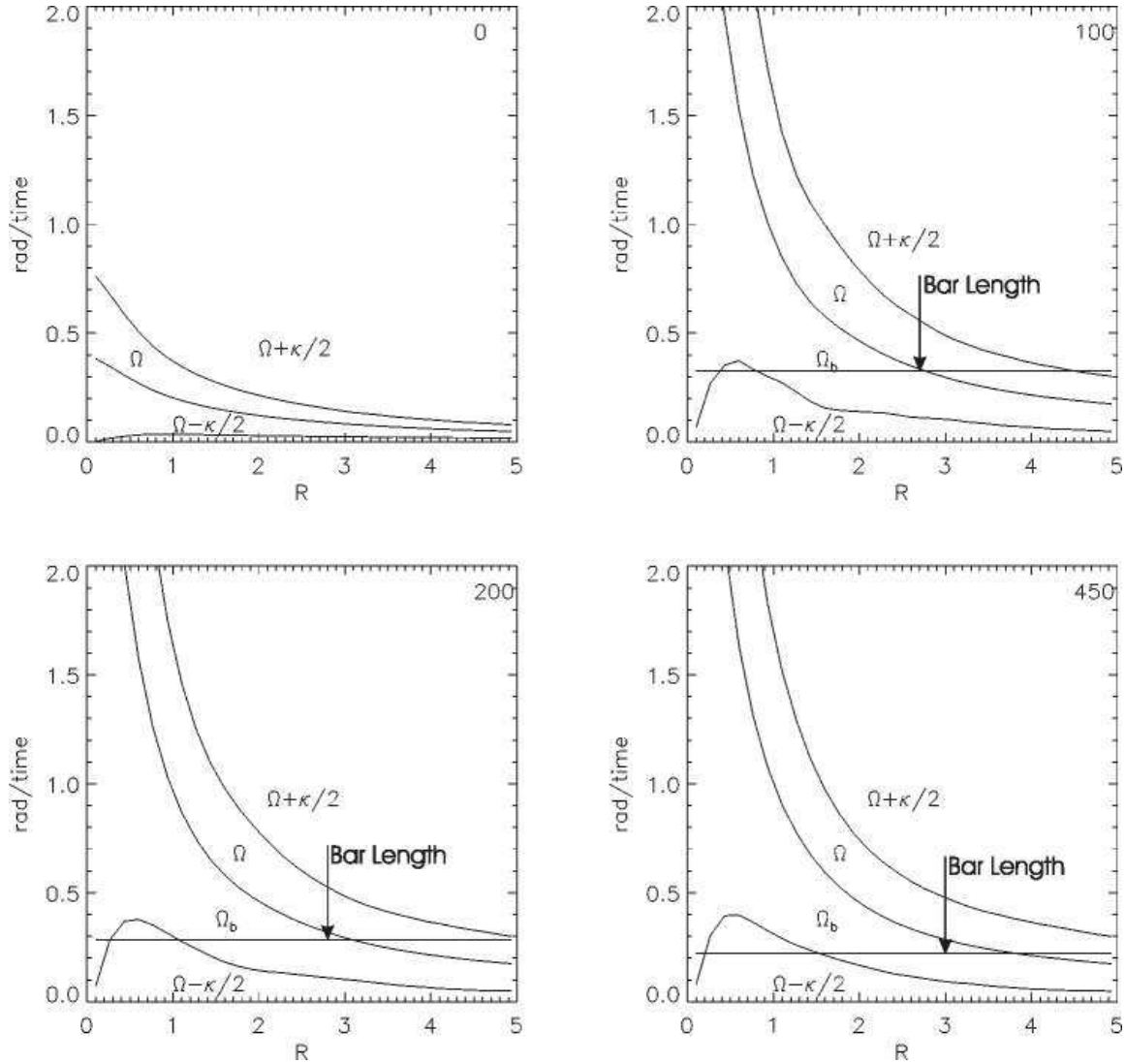


Figure 15. Lindblad resonances and the bar pattern speed for $t=0, 100, 200$, and 450 . In all cases the bar is slow; at $t=450$ the bar length is around a scale length and within the ILR as predicted for late-type barred spirals by Elmegreen and Elmegreen (1985)

mesh is most likely the reason for the disparity. The higher resolution leads to stronger forces in the central region of the galaxy, which the initial velocity dispersion does not support, causing a slight collapse of the disc particles to the centre at the beginning of the simulation. This causes the rotation curve to rise more steeply, which leads to a shorter bar (Combes & Elmegreen 1993). The shorter bar feels less friction from the halo, which results in less pattern speed deceleration and the higher pattern speeds found here.

Run 68 in D&S was actually conducted with a $Q=0.05$ model. Due to earlier attempts on our models, we were concerned about the low Q value and the stability of the disc. We were unsuccessful in reproducing the output from this model, as we were in our own discs with a Q much below 1.0. Their results may be due to the way the particles were set up in relation to their grid, or the grid method may be supplying some artificial stability to the model.

A copy of our low resolution initial conditions were also forwarded back to Debattista and Sellwood. Using a new hybrid grid code with softening of $0.025R_d$ and a time step of

0.025 they found bar lengths between 2.5 and 3, well within the error bars of Fig. 11. They measured the strength of the bar by calculating the $m = 2$ amplitude of the whole disc as a function of time. The resulting strength is very similar to ours for the same resolution, however we find a greater bar strength for the 20M run between $t = 150$ and $t = 450$. The increase may be due to the larger number of particles available for angular momentum transfer in that model. Although we agreed well until $t = 150$, they found a significantly higher pattern speed thereafter, as their simulation did not slow down as much as ours. The reason for this is unclear at the moment.

While initial differences were seen, the comparison between these codes has shown most of the results to be reproducible. That said, direct code comparison is very much needed in this field to determine the influence of method versus initial conditions.

10 CONCLUSIONS AND FUTURE WORK

The three N-body galaxy models created here generally concur with previous research in structure (face-on and edge-on shapes of bars).

The bars measured here are all fast, with pattern speeds in the range of those observed directly in early-type galaxies. Although the pattern speeds of late-type galaxies, which would be a more appropriate comparison to these simulations, cannot be directly measured, kinematical studies have agreed that their bars are also fast (e.g. van Albada & Sanders 1982; Hunter et al. 1988; Athanassoula 1992; Lindblad et al. 1996; Weiner et al. 2001).

The corotation to bar axis ratio in the high resolution simulation is less than 1.5, which is designated a fast bar. This is marginally consistent with the D&S simulations, although our models did not require a fully maximal disk to remain fast.

A recent preprint by Valenzuela & Klypin (astro-ph/0204028) outlined a simulation which used 780K particles (model B), Hernquist initial conditions, and an adaptive tree-mesh code that has a higher resolution at the centre than the less active outer regions. Their spatial resolution in the central regions is slightly lower than ours, and they use many fewer particles than our high resolution model. Many of their results are in agreement with those presented here: namely, comparable angular momentum transfer, the central density build up created by the bar and its affect on the rotation curve, the lack of alteration of the dark matter density distribution, and the double exponential disk density profile. We disagree in bar length (theirs are much shorter), actual pattern speed (they find a more rapid rotation), and pattern speed degradation (their pattern speed is constant). Our disc to halo mass ratio and Q parameter are different, though, which may account for some of the discrepancies.

By comparing our 20M particle simulation with a 500K particle model, it was determined that the basic dynamics of the system can be reproduced with lower resolution (pattern speed, overall evolution), but if observational techniques are to be used on the results, higher resolution is needed. The techniques used to varying degrees of success here were the T&W method to find pattern speed and the K&M edge-on line-of-sight velocity distribution plots to find bar orbits.

The results presented here agree with much of the previous work done on isolated, bar unstable galaxy simulations. We have shown resolution is no longer a large source of error. We suggest further investigations should concentrate on generating early-type barred spiral galaxies with high resolution low softening codes. Also, more observational data of real pattern speeds, especially for late-type galaxies, would be a great asset to the field.

11 ACKNOWLEDGMENTS

We would like to acknowledge the assistance of Victor Debattista, Jerry Sellwood, and the anonymous referee for detailed and thought provoking comments, as well as the NSERC and the Canadian Foundation for Innovation.

REFERENCES

- Abraham R.G., Merrifield M.R., Ellis R.S., Tanvir N.R., Brinchmann J., 1999, MNRAS, 308, 118
 Athanassoula E., 1992, MNRAS 259, 345
 Athanassoula E., 2002a, ApJ 569, L83
 Athanassoula E., 2002b, in Athanassoula E., Bosma A., Muijica R., ed., ASP Conf. Ser. Vol. 275, Disks of Galaxies: Kinematics, Dynamics and Perturbations. Astron. Soc. Pac., San Francisco, p. 141
 Athanassoula E., Bureau M., 1999, ApJ 522, 699
 Athanassoula E., Misiriotis A., 2002, MNRAS 330, 35
 Bureau M., Athanassoula E., 1999, ApJ 522, 686
 Bureau M., Freeman K.C., Pfizner D.W., Meurer G.R., 1999, AJ 118, 2158
 Combes F., Elmegreen B.G., 1993, A&A 271, 391
 Combes F., Sanders R.H., 1981, A&A 96, 164
 Debattista V.P., Corsini E.M., Aguerri J.A.L., 2002, MNRAS 332, 65
 Debattista V.P., Sellwood J.A., 2000, ApJ 543, 704
 deVaucouleurs G., 1963, ApJ 8, 31D
 Dubinski J., 1996, NewA 1, 133
 Dubinski J., Carlberg R.G., 1991, ApJ 378, 496
 Elmegreen B.G., Elmegreen D.M., 1985, ApJ 288, 438
 Eskridge P.B. et al., 2000, AJ 119, 536
 Gerssen J., Kuijken K., Merrifield M.R., 1999, MNRAS 306, 926
 Hernquist L., 1993, ApJS 86, 389
 Hunter J.H.Jr., England M.N., Gottsman S.T., Ball R., Huntley J.M., 1988, ApJ 324, 721
 Kent S.M., 1986, AJ 91, 1301
 Kent S.M., 1990, AJ 100, 377
 Kent S.M., Glauddell G., 1989, ApJ 98, 1588
 Kuijken K., Dubinski J., 1995, MNRAS 277, 1341
 Kuijken K., Merrifield M.R., 1995, ApJ 443, L13
 Lindblad P.A.B., Lindblad P.O., Athanassoula E., 1996, A&A 313, 65
 Merrifield M.R., Kuijken K., 1995, MNRAS 274, 933
 Merrifield M.R., Kuijken K., 1999, A&A 345, 47L
 Misiriotis A., Athanassoula E., 2000, in Combes F., Mamon G.A., Charmandaris V., ed., ASP Conf. Ser. Vol. 197, Dynamics of Galaxies: from the Early Universe to the Present. Astron. Soc. Pac., San Francisco, p. 69
 Navarro J.F., Frenk C.S., White S.D.M., 1996, ApJ 462, 563
 Navarro J.F., Frenk C.S., White S.D.M., 1997, ApJ 490, 493
 Norman C.A., Sellwood J.A., Hasan H., 1996, ApJ 462, 114
 Ostriker J.P., Peebles P.J.E., 1973, ApJ 186, 467
 Pfenniger D., Friedli D., 1991, A&A 252, 75
 Raha N., Sellwood J.A., James R.A., Kahn F.D., 1991, Nature 352, 411
 Sellwood J.A., 1981, A&A 99, 362
 Sellwood J.A., 1997, in Clarke D.A., West M.J., eds., ASP Conference Series 123, Computational Astrophysics, p. 215
 Sellwood J.A., Wilkinson A., 1993, Rep. Prog. Phys. 56, 173
 Shaw M.A., Combes F., Axon D.J., Wright G.S., 1993, A&A 273, 31
 Tremaine S., Weinberg M.D., 1984a, MNRAS 209, 729
 Tremaine S., Weinberg M.D., 1984b, ApJ 282, L5
 Valenzuela O., Klypin A., 2002, astro-ph/0204028
 van Albada T.S., Sancisi R., 1986, Phil. Trans. R. Soc. Lond. 320, 447
 van Albada T.S., Sanders R.H., 1982, MNRAS 201, 303
 Weinberg M.D., 1985, MNRAS 213, 451
 Weinberg M.D., 2001, MNRAS 328, 311
 Weinberg M.D., Katz N., 2002, ApJ 580, 627
 Weiner B.J., Sellwood J.A., Williams T.B., 2001, ApJ 546, 931

This paper has been produced using the Royal Astronomical Society/Blackwell Science L^AT_EX style file.